Effect of bending rigidity on gel mechanical response

Patrick Soltis, Candidate for B.S. in Biological Physics
Advised by Dr. Emanuela Del Gado

Abstract

Gel-like materials are ubiquitous in modern manufactured products, the human body, and food. Further advanced applications of gels require producing gels with finely tuned mechanical responses. However, such tuning requires an understanding of how these responses originate in the microscopic properties of the gel's molecular network, such as the bending rigidity of gel network branches. This investigation relies on 3D computer simulations to study how the bending rigidity affects a gel's mechanical response to shear strain. Increased bending rigidity decreases both the critical strain at which the gel's load curve switches from linear to nonlinear, as well as the yield strain. Overall, the nonlinear regime becomes shorter. This is similar to the effects of increased network density, likely because both bending rigidity and high density restrict the network's ability to rearrange in response to deformation. In addition to the supporting data, this text describes the main physical properties of the soft gels that motivated the study, the numerical approach taken to simulate the gel, and important questions to investigate in further studies.

Introduction

A. Soft matter and gels

Many of the materials that dominate problems in manufacturing and medicine in the 21st century cannot be described as simply "liquid" or "solid", but as something in between, having a combination of properties from both groups. Generally, these materials are known by such terms as "soft matter" and "complex fluids".[1,2] A common characteristic of soft matter materials is that their structural units are large compared to atoms. (Classical solids, by contrast, typically are crystalline arrangements of single ions.[3]) At room temperature, soft matter typically exhibits a response to weak forces that is non-linear and rather large relative to the force.[2,4] The relative ease of deformation renders the feeling of softness.

The non-linear response of soft matter adds a layer of complexity that must be understood in order to develop materials for industrial, medical, and gastronomical uses with specific characteristics. One type of complex fluid is a gel. Structurally, a gel is a network of polymers, particles, or fibers with a solvent trapped inside the network.[5,6] Functionally, such materials can change from solid-like to liquid-like behavior under deformation.[1] They can be deformed large amounts before breaking, or can even self-heal upon breaking.

B. Designing better gels

Gels are everywhere in our world. Naturally occurring gels include networks of collagen and actin, which make up, respectively, the extracellular matrix and cellular cytoskeleton of most animals, including humans.[7–10] Synthetic gels constitute a wide variety of materials integral to the functioning of society, including cement, as well as a number of foods integral to some diets, such as yoghurt, jellies, and gelatin desserts.[11,12] Like gels, rubbers also contain a complex polymer or fiber network, and so the theory of rubber elasticity is also applicable to gels.[13] The major

difference between a gel and a rubber is that a solvent is typically trapped within a gel's network, while a rubber's network is so dense that it does not contain any solvent.[6]

Gels are a class of material that can provide a continually widening range of practical uses. Self-healing materials investigated in laboratories, for example, are being developed to function in a wide range of environments, allowing for uses in automotive design, household appliances, and packaging.[14,15] As the human body is replete with gel-like substances, development of biotechnology requires inventing a variety of gels with physical properties that will interface appropriately with living tissue.[16–18]

In order to create such materials, a rigorous understanding of the gel's microscopic structure is required, as this structure determines gel mechanics to a large degree. Microscopic network properties such as local density, bond angle, local stiffness, connectivity, and morphology define the material structure which collectively entails the material's macroscopic behavior. In order to develop new gels having the specific behavior required for a particular medical or industrial use, one must understand what particular properties of the molecular network correspond to these desired macroscopic properties.[19] This relationship is not well understood.[20] Such an understanding also applies to existing biological materials studied in medicine, such as collagen and actin. A deeper microscopic understanding of collagen and actin networks would allow doctors and biomedical engineers to target an important pathway for the mechanical failings of cells, organs, and other tissues.[21–24]

C. Strain and stress tensors

The mechanical response properties of any material can be characterized in terms of stress and strain, each one requiring a tensorial description.

A material can be modeled as a continuous medium that is divisible into discrete volume elements. The position of each volume can be described by its center of mass. The position of any volume element may change when the material of the body is deformed.

The displacement vector u represents the displacement of a given volume element due to deformation:

$$u_i = x'_i - x_i$$

where x is the position of the element's center of mass before the deformation and x' is the position after. The subscript i refers to one of the three components of dimension in Euclidean space (e.g. x, y, or z).

The strain tensor is an operator that relates the displacement of the volume element to the initial position of the volume element. Each component of the strain tensor u_{ij} shows how the position in the i-component (x_i) of a given point particle changes with respect to changes in the j-component. This relationship is given by

$$u_{ij} = u_{ji} = \frac{1}{2}\left(\frac{\partial u_i}{\partial x_j} + \frac{\partial u_j}{\partial x_i}\right)$$

and holds for small deformations.[25]

Internal forces act at the interface between every two adjacent volume elements. These are actually the forces acting between microscopic units of the material on opposite sides of the given interface. In amorphous solids, there may be internal forces balanced between these volume elements since the microscopic units sit at local but not absolute minima of their total potential of free energy. When the material is strained, displacing the microscopic units alters their potential energy, causing changes in the forces between the volume elements.

Each component of force (F_i) on a given volume element can be written as a surface integral over the surface area:

$$\int F_i dV = \oint \sigma_{ij} df_j$$

where σ_{ij} is a component of the stress tensor and df_j is the portion of the surface area normal to $\hat{\jmath}$. The relation directly above is valid for all possible combinations of F_i and df_j, meaning that σ_{ij} defines components of the stress tensor for every such combination.[25] While I can compute the whole stress tensor, in the following I focus on its shear component.

D. Rheology

Rheology is the study of flow and deformation, measuring the viscosity and elasticity of the material in question.[26] Experiments may apply strain and measure resulting stress, and vice versa. Our simulations model the former process.

An instrument which takes rheological measurements is known as a rheometer. In the most common experimental systems, strain is applied by spinning a plate on the surface of a sample of the substance while the surface supporting the substance from below remains stationary or spins in the opposite direction (Fig. 1a). This applied strain is shear strain, denoted as γ_{xy}, where x is the axis along which the deformation is applied and y is the axis normal to the surface along which the deformation is applied. This type of deformation is easiest to apply in a controlled manner, and the resulting shear component of strain (σ_{xy}) is most convenient to measure. The reverse (i.e. applying stress and measuring the resulting strain) can also be done, though my measurements center around the former. Much rheological data quantifies relationships between shear stress and shear strain.

While the spinning plate method shown in Figure 1a provides helpful measurements of mechanical response over a uniform gap (h), different shapes of instruments are required for testing multiple values of h at once or measuring normal stress differences. A cone and plate arrangement, as shown in Figure 1b, is a more popular choice because the geometry of a cone can test those variables.[1]

This investigation makes measurements exclusively of shear stress and shear strain. Unless otherwise noted, assume henceforth that a symbol for strain (γ) or stress (σ) refers to its shear component. The shear strain is defined as

$$\gamma(t) = \frac{d(t)}{h}$$

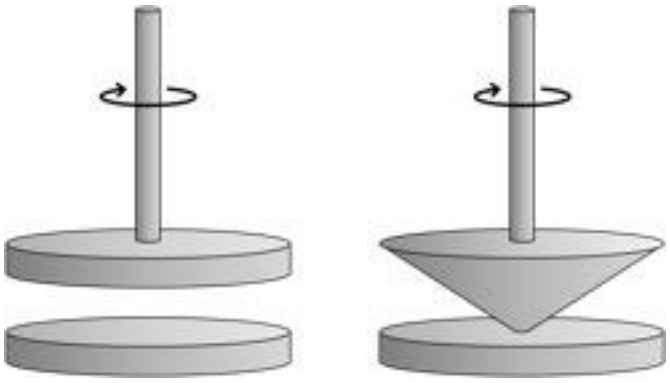

Figure 1. *Different geometries of rheometers. (a, left) The plate-plate method creates strain across a sample of uniform depth h. (b, right) The cone and plate method is more versatile and allows for testing of multiple sample depths at once. The rotational nature of both designs lends itself handily for oscillatory patterns of strain. Borrowed from Ref. 27.*

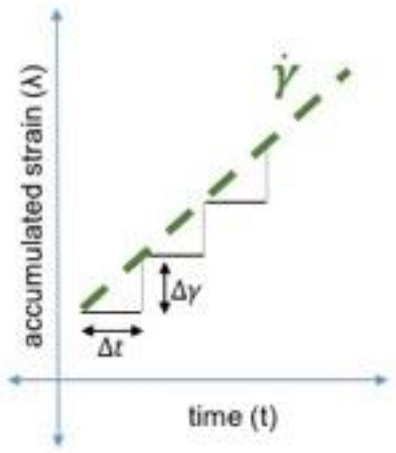

Figure 2. *Step strain describes a process by which strain accumulates in discrete bursts of Δγ (vertical line segments), each burst separated by a time interval of Δt (horizontal line segments). When Δγ and Δt are sufficiently small, the staircase shape can be abstracted to a line of slope Δγ/Δt (green dotted line), which represents the strain rate $\dot{\gamma}$.*

where h is the depth of the substance and $d(t)$ is the distance that any point on the plate has traveled over time t.[6] The shear stress is computed as the average of σ_{xy} across all volume elements in the sample.

I will consider the strain to be applied in a stepwise manner. The accumulated step strain $\gamma(t)$ is defined as[26]

$$\gamma(t) = \sum_i \Delta\gamma_i \Theta(t - t_i)$$

where i is an index for every step in the function. t_i is thus the time at which step i occurs, and $\Delta\gamma_i$ is the amount of strain (i.e. the "height" of the step) that is added at t_i. Our simulation features both a $\Delta\gamma_i$ and Δt_i that remain constant through the simulation. Since the two quantities are independent of the specific i, they are henceforth written as $\Delta\gamma$ and as Δt. In simulations, the box containing particles is deformed instantaneously with the intended $\Delta\gamma$, forcing the particles within to adjust. This deformation is followed by a period of time Δt in which no strain is applied (Fig. 2).

When both $\Delta\gamma$ and Δt are sufficiently small, the accumulated step strain can be described by a single, continuous line connecting the front edges of the staircase formed by $\Delta\gamma$ and Δt (Fig. 2). This line represents the strain rate. Strain rate is defined as

$$\dot{\gamma} = \frac{\Delta\gamma}{\Delta t}$$

where Δt is the time between steps. A change in strain rate can be effected by changing either $\Delta\gamma$ or Δt. When there is a linear relationship between stress and strain, the slope of the line describing this relationship is dependent on the strain rate. A relationship between the stress and strain of a material is known as a load curve.

In a simple elastic materials, the shear stress is linearly related to shear strain by the shear modulus G:[26]

$$\sigma = G\gamma$$

In soft matter such as gels, however, the relationship is more complicated.[19] Typically, the gel load curve exhibits such a linear relationship at low strains, but the stress begins to increase exponentially beyond a certain level of strain (Fig. 3). This critical strain is denoted by γ_c. The shear stress at γ_c is denoted by σ_c. I use these quantities to characterize the model gel's mechanical response.

Because the load curve becomes nonlinear at higher strains, the shear modulus *G* cannot describe the function across all relevant strains. The differential modulus, *K*, is a parameter that can describe the form of a load curve outside the confines of a linear relationship. While a differential modulus can be made from any component of strain and of stress, here I mean the shear modulus, in which both the strain and stress considered are shear components:

$$K = \frac{d\sigma}{d\gamma}$$

The nonlinear regime is understood as a regime of material stiffening, known as strain stiffening.[27]

This regime can be characterized by the exponent α, extracted from a best fit curve over the nonlinear portion with the form:

$$K = A\sigma^{\alpha}$$

The exponent is an indicator of the material's performance, as a larger α means that the material exhibits a stronger internal stress reaction to strain. This is an important characteristic of mechanical response, as a more quickly aggregating stress response may render a material unstable under rapid strain. Common biopolymers show clear variation in this exponent: while α=1 for collagen, the main component of the extracellular matrix, α tends towards 3/2 for actin and intermediate filament networks which scaffold the interior of the cells.[27] *A* is an arbitrary constant.

As with a simple elastic material, a gel will reach a maximum strain after which the material will yield or break. This maximum strain that the gel can support is the yield strain γ_{max}. Obviously, the yield strain is an extraordinarily relevant property for materials development. After a gel passes the yield strain, it is no longer elastic, and a material that is expected to

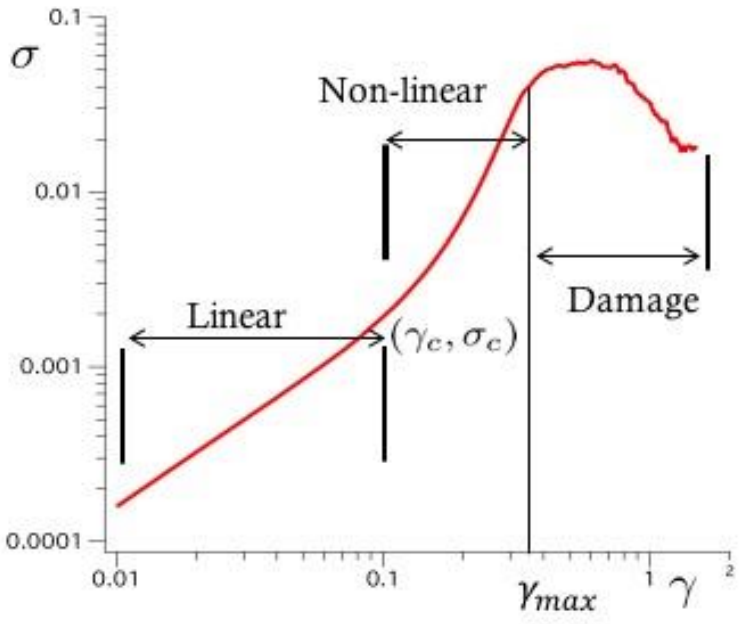

Figure 3. *Load curve of a typical gel. A load curve shows stress (σ) as a function of strain (γ). I use mainly shear components of both stress and strain. At low strains, a gel exhibits a linear elastic response, where strain is related to stress by the shear modulus G: $\sigma = G\gamma$. At higher strains, the curve transitions into a nonlinear strain stiffening regime. The strain at which the load curve transitions between linear and nonlinear is known as the critical strain (γ_c), and the exhibited stress is known as the critical stress (σ_c). At even higher strains, the material yields and the load curve ceases to follow a significant form. Image borrowed from Ref. 36.*

maintain elastic properties would majorly disappoint if conditions in its environment take it past the yield strain.

E. Microscopic properties

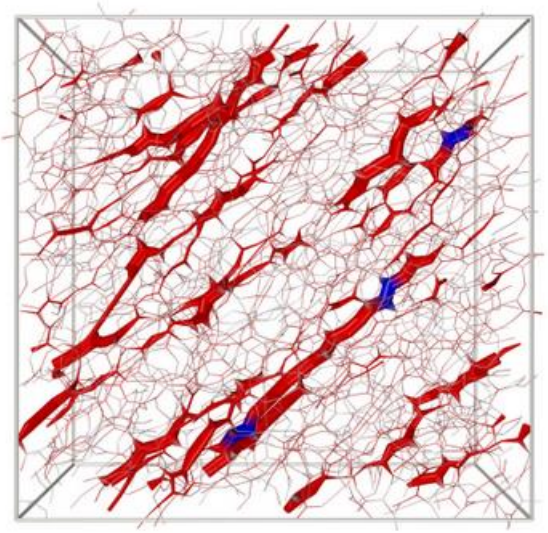

Figure 4. *A snapshot of a gel network under shear strain. Only bonds are shown, and thicker strands show bonds that are subject to a disproportionate amount of stress. Blue indicates where breaking will happen. Image borrowed from Ref. 30.*

The nonlinear regime is known to result from two phenomena in gel network structure.[28] First, stresses in deforming gels progressively align to the extensional axis of shear (45°) as shear strain accumulates. Not coincidentally, orientation of filament chains (a chain being a series of gel branches that are connected end to end in a single, non-divergent strand) corresponds to this progressively aligning stress. This occurs because the space between the top and bottom surfaces of the gel is increasing, creating a need for joints in the filament branches to unbend to achieve their longest possible configuration, which is by definition where they are connected end-to-end in a straight line. Second, once these chains are unbent to their maximum length, the deformation pulls at the filament branches themselves. The stress is concentrated in these chains, meaning that the resistance to deformation is heavily concentrated in a few parts of the structure (Fig. 4). The intense stress leads these chain segments to break, which triggers the yielding of the entire gel since the gel depends largely on those few chains to bear the stress of the deformation. The point at which these chains break is the yield strain γ_{max}, i.e. where the nonlinear regime ends. Each filament branch can be thought of as a bond between two gel particles. Bonds break and new bonds form before γ_{max}, but after γ_{max} the rate of newly broken bonds exceeds the rates of newly formed bonds, causing an overall decrease in the number of bonds. Although slower shear rates allow more bonds to reform after γ_{max}, the strength of the material does not recover since these bonds are formed in such a way that they are not capable of bearing further stress.[19]

The form of the nonlinear regime depends on the balance between stretching and bending modes of the filament network. A stretching mode refers to the elastic resistance of a single filament branch to deformation when it is pulled. A bending mode refers to how the bending or unbending of a joint between two filament branches either contributes to or resists deformation.[27]

Density of the gel network affects the balance between the stretching and bending modes, which in turn affects the size and form of the nonlinear regime. In all cases, stretching modes resist the deformation, since any filament branch spanning a structure that is pulled apart will work to hold the structure together until the branch yields. Bending modes vary, however. At low densities, stretching modes resist the deformation while bending modes favor the deformation. A 3-body potential term makes it energetically more favorable for two bonds on a single particle to be directly opposite each other. The only thing keeping this from happening would be a third bond

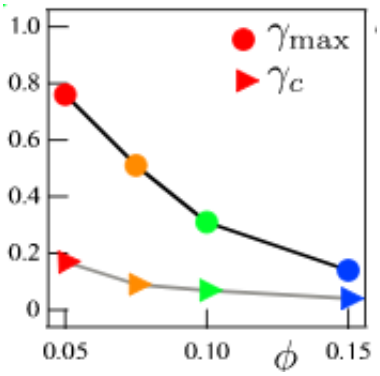

Figure 5*. Changes in γ_{max} and γ_c as a function of number density. Borrowed from Ref. 19.*

keeping the joint from unbending, similar to a finger holding back a bowstring to keep it from tightening under tension from the bow. At low number densities (e.g. 5%), there are few extra particles nearby to create this third bond, permitting many initial filament branch joints to use the deformation as an opportunity to achieve the lower-energy state of a straight chain link. The relaxed bending modes allow the gel to somewhat soften before the overstretched chains break and cause the gel to yield. In this case, the stretching and bending modes balance each other until yielding, resulting in a prolonged nonlinear regime (Fig. 5).[19]

At higher densities (e.g. 10%), the bending modes are overcome by the stretching mode, causing the gel to stiffen instead of soften. The higher density means there are more 3-bond particles, henceforth referred to as nodes, which prevent the bent filament joints from unbending to relieve their stress. The brunt of the stress resulting from the deformation is thus borne by the stretching mode. There is still enough space, however, that there are plenty of chains (although fewer than with 5% density) on which the stress can accumulate before those filament chains yield.[19]

At even higher densities (e.g. 15%), there is little space for the filament chains to develop since a more crowded space requires a higher amount of bonds between particles in close quarters, and thus many nodes. As a result, the deformation does not allow the filament joints an opportunity to relieve their stresses, as there are too many "third" bonds locking the branches of the filament joints in place. Thus, with few chains to bear the brunt of the deformation, the stress is more evenly distributed throughout this gridlocked network of gel branches. The system is able to bear greater amounts of stress since more of the branches are able to resist the deformation. However, the dense, gridlocked system contains few opportunities for structural readjustment in response to the deformation, causing the system to quickly stiffen and break. Because the joints cannot unbend in the direction they please, the bending modes join the stretching modes in resisting deformation. Hence the nonlinear regime is limited for high densities, meaning a quick transition between the linear, elastic regime and the yielding regime (Fig. 5). Due to this even distribution of stress, more branches become overstressed at the same time, leading to a higher number of bonds breaking immediately at γ_{max}.[19]

The form of the nonlinear regime, not just its size, is also important. As mentioned above, α is the exponent that characterizes the nonlinear regime. At high strains, the gel load curves display a nonlinear regime similar to the biopolymer actin. However, the biopolymer collagen shows a linear dependence (α=1) even for high strains. What gives the two biopolymers, each of which compose major portions of living organisms, such different properties? There are potentially two separate components of the nonlinear regimes: the low strain regime (following the linear, elastic portion), which is dominated by bending modes, and the high strain regime (directly preceding yielding) which is dominated by stretching modes. The linear regime observed in collagen has the appearance of the low strain, bend-dominated regime without ever transitioning to the high strain, stretch-dominated one.[27] Some quality of the polymer collagen may prevent stretching modes from becoming significant even at high strains. The origin of the nonlinear regime in general could be explained by entropic contributions to free energy in the system thanks to the increased heterogeneity afforded by the gel branches' flexibility.[19] Moreover, separate models for simulating

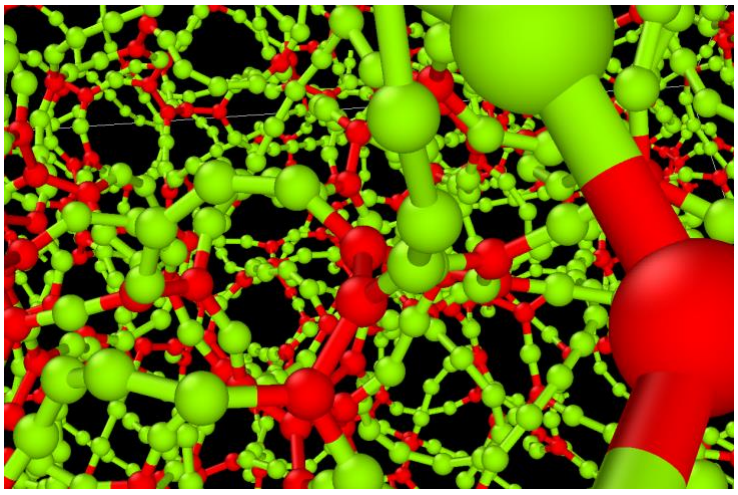

Figure 6*. The inside of a simulation is visualized. Spheres represent particles and the rods between them represent bonds. Green particles are those with a coordination number of 2, while red particles have coordination 3.*

gels also show a similar variation in α values. While simulations using the featured show α falling between 1 and 3/2, investigations using another popular model show α falling between ½ and 1.[7,19] Since competing stretching and bending modes could potentially explain the discrepancy between collagen (α=1) and actin (α=3/2), perhaps this same competition could explain the discrepancy between the other model (α=1) and the featured model (α=3/2).

Familiar with the sensitivity of the nonlinear regime to the two modes, I supposed that altering the balance of the bending and stretching modes could be an effective mechanism for controlling the mechanical response of a gel. In this investigation, I alter the bending rigidity of the filament joints and assess the effect that this changed rigidity has on the gel's mechanical response. During the preparation of gels, chemical and thermal mechanisms can be leveraged to alter bending rigidity of the filament joints. Previous experiments show a range of interesting effects that correlate to changes in bending rigidity.[4,8,29–31] I elaborate, in general terms, how bending rigidity influences the ability of a gel to bear stress at a microscopic level. I analyze the effects of changes in bending rigidity on the mechanical response, as well as on easily measurable network properties such as coordination number. I then comment on these effects using the framework of previous simulations and experiments.

The coordination number ($\mathbb{C}$) of a particular particle indicates the number of other particles to which a given gel particle is bonded. The coordination number in the simulations range from 0 to 4, though 2 and 3 are predominant (Fig. 6). Particles with $\mathbb{C} = 2$ are described as chain links and particles with $\mathbb{C} = 3$ are described as nodes. While $\mathbb{C} = 2$ and $\mathbb{C} = 3$ particles each have a special role in bearing deformation, tracking the change in relative distribution between the two is a useful way to count the change in total bond number and thus the point at which bonds break or form.

Methods

This investigation tests the mechanical response of gels in a numerical model. I model an abstracted, generic gel: all distance is measured in terms of particle diameter, all energy is measured in terms of a constant ϵ in the interactive potential function, and all time measured as a function of particle diameter and ϵ. The model and the numerical methods do not reproduce all the details of the experimental studies, admittedly. However, this allows us to disentangle the fundamental physical mechanisms at play in a general gel structure, as well as their effect on the mechanics, from properties specific to certain types. The gel microscopic units are represented as particles interacting through potential attraction and repulsion.

A. Model

The gel microscopic units are represented as particles interacting with a potential defined by

$$U(\boldsymbol{r_1}, \ldots, \boldsymbol{r_N}) = \epsilon \left[\sum_{i>j} u_2\left(\frac{\boldsymbol{r_{ij}}}{d}\right) + \sum_{i} \sum_{j>k}^{j,k\neq i} u_3\left(\frac{\boldsymbol{r_{ij}}}{d}, \frac{\boldsymbol{r_{ik}}}{d}\right) \right]$$

- N is the number of particles
- $\boldsymbol{r_i}$ is the position vector of particle i, where i goes from 1 to N
- $\boldsymbol{r_{ij}} = \boldsymbol{r_j} - \boldsymbol{r_i}$
- ϵ is the energy scale of the system, the depth of the attractive well, typically 1-100 $k_B T$ for colloidal particles in aqueous solutions
- d is the particle diameter, typically 10-100 nm for a colloidal system
- u_2 is a function (defined below) describing the attractive and repulsive interactions between two given particles
- u_3 is a function defining angular rigidity between bonded particles

u_2 describes a typical potential interaction between two particles, changing as the distance between them ($\boldsymbol{r_{ij}}$) changes. The u2 term closely corresponds with the stretching mode. The potential reaches a minimum when $r_{ij} = r^*$, an energetically favorable distance at which the particles are bonded. The potential then sharply increases as the particles get closer, i.e. as $r_{ij} \rightarrow 0$ (Fig. 7).

$$u_2(r) = A(ar^{-18} - r^{-16})$$

where A and a are constants, set to 23 and 18. The 3-body term u_3 describes angular rigidity of a given filament joint, where **r** and **r'** represent the bonds that make up the joint, vectors originating at the particle at the vertex of the angle (Fig. 8).

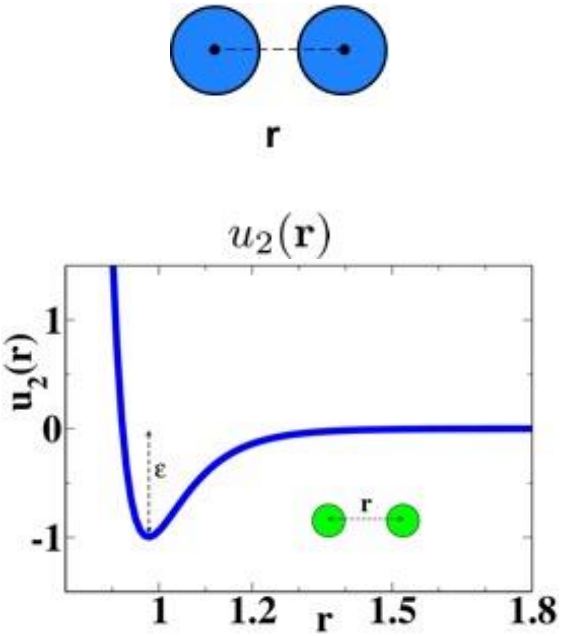

Figure 7. *Illustration of the 2-body potential term (u_2).* ***Upper.*** *The distance between the center of two particles are separated by the distance r.* ***Lower.*** *A plot of the u_2 term with respect to r holding all else constant.*

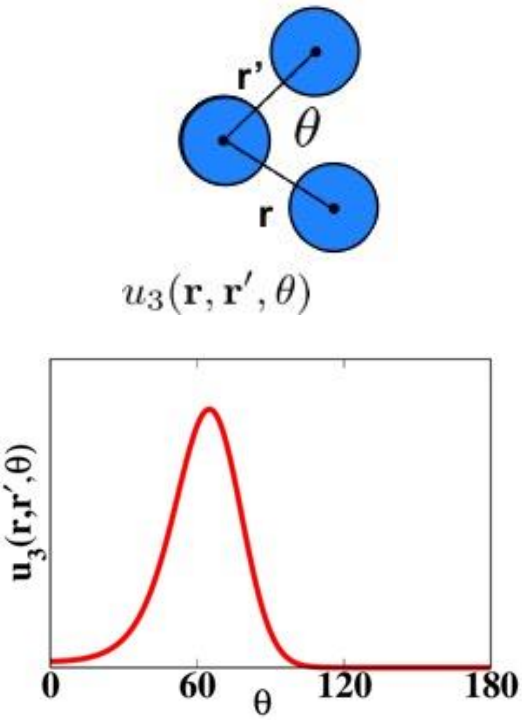

Figure 8. Illustration of the 3-body potential term, u_3. ***Upper.*** *A third particle is considered at a distance r' from the initial two particles. The center particle bonds to the nearby particles, the bonds forming the angle θ.* ***Lower.*** *A plot of the u_3 term with respect to θ holding all else constant. The maximum value of u_3 occurs when $\theta = \bar{\theta}$.*

$$u_3(\boldsymbol{r}, \boldsymbol{r'}) = B\Lambda(\boldsymbol{r})\Lambda(\boldsymbol{r'})e^{-\left(\frac{\boldsymbol{r}\cdot\boldsymbol{r'}}{rr'} - \cos\bar{\theta}\right)^2/w^2}$$

The u_3 term closely corresponds to the bending mode.

I single out $\bar{\theta}$ as a parameter that can change the bending rigidity.[a] For a given pair of adjacent bonds **r** and **r'** at a fixed angle, $\bar{\theta}$ is a value at which $\exp\left[-\left(\frac{\boldsymbol{r}\cdot\boldsymbol{r'}}{rr'}-\cos\bar{\theta}\right)^2/w^2\right]$ hits its maximum of 1, making $u_3 = B\Lambda(\vec{r})\Lambda(\vec{r'})$.[b] This occurs when the angle (call it θ) between **r** and **r'** is equal to $\bar{\theta}$. Deviation of θ from $\bar{\theta}$ causes a decrease in the u_3 term whether θ is at a larger or a smaller angle than $\bar{\theta}$ (Fig. 8). Angles larger than $\bar{\theta}$ decrease u_3, simulating a reduction in repulsion as the angle between **r** and **r'** widens. A decrease in u_3 at smaller angles seems counterintuitive since tighter bending should equate to a higher energy cost. However, this energy cost is accounted for in the u_2 term since, as the angle gets tighter, the particles on the outside of the joint angle will be approaching and thus experiencing the repulsion of this two-body potential. Changing $\bar{\theta}$ changes the value of θ that will max out the u_3 term: progressively higher $\bar{\theta}$ values increases this maximum θ, causing this least preferred angle to become wider and wider, inducing filament joints to remain at wider angles (Fig. 9). [19,28,32,33] I keep $\bar{\theta} < 90°$, low enough that there is no safe zone of energetically preferred angle values less than $\bar{\theta}$. In 3 dimensions for particles each hosting no more than 3

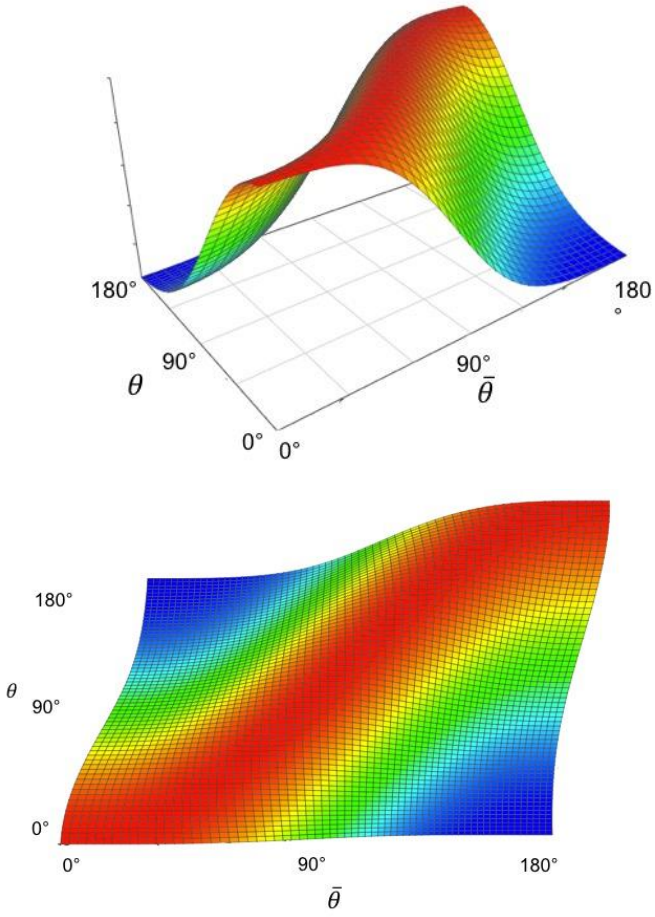

***Figure 9**. Intensity of u_3 term for a specific filament joint at varying values of θ and $\bar{\theta}$. **Upper.** The maximum value of u_3 is achieved when of $\theta = \bar{\theta}$. u_3 decreases from the maximum as θ gets either higher than or lower than $\bar{\theta}$. **Lower.** View of the plot from above, i.e. looking at the $\theta\bar{\theta}$-plane. Red indicates highest u_3, followed by yellow, green, and blue.*

[a] *B* can also be altered to change the bending stiffness. This would change the strength of the entire u_3 function relative to u_2, which has different physical implications than altering $\bar{\theta}$. That difference is beyond the scope of this investigation.

[b] For this simulation, $B = 10$. $\Lambda(r)$, the radial modulation, ensures that the 3-body interaction only exists at distances of less than two particle diameters. The radial modulation term is defined as:

$$\Lambda(r) = \begin{cases} r^{-10}\left[1-(r/2)^{10}\right]^2 & r < 2 \\ 0 & r \geq 2 \end{cases}$$

bonds, bond angles would rarely or never be less than 90°. Note that this means, in practicality, no θ will match the current value of $\bar{\theta}$.

In this simulation, bonds are generated between two particles whenever the distance between them is within a defined "bond length". Bonds are not computed while the simulation runs.[c] Rather, they can be added when the particle coordinates are visualized (Fig. 6) or computed by a script that identifies the distance between every pair of particles. A bond length must be set to match the r^* arising from the u_2 term. When any $|\boldsymbol{r_{ij}}(t_1)| \leq r^*$, $\boldsymbol{r_{ij}}(t_1)$ represents a bond. (If $|\boldsymbol{r_{ij}}(t_2)| > r^*$ even after $|\boldsymbol{r_{ij}}(t_1)| \leq r^*$, $\boldsymbol{r_{ij}}(t_2)$ will not be a bond.) In our simulations, r^* = 1.3 (in units of particle diameter), consistent with earlier experiments using this model.[19]

In this model, gels are prepared by heating and rapidly cooling a system of N identical particles. Beginning with particles on an fcc lattice at a specified density, system energy ($\frac{k_B T}{\epsilon}$) is held at 1 for an interval of time that varies by simulation. The high temperature provides extreme thermal energy to randomize the initial positions of the particles. This varying length of time allows for the creation of multiple systems having equivalent macrostates but unique microstates. $\frac{k_B T}{\epsilon}$ is then steadily decreased from 1 to 0.05 over a short period of time (constant across all simulations), then kept at 0.05 for an equivalent interval of time. The high thermal energy (where $k_B T = \epsilon$) disrupts and melts the crystalline lattice of particles. The subsequent cooling drives the particles' aggregation into a disordered gel network.

In the simulations, N is fixed by the volume of the system (V) and the number density ($\rho_\# = N/V$). In this investigation, $N = 4 \times 10^3$. The number density $\rho_\# = N/V$ is fixed in each simulation and I translate it into a volume fraction by considering that the volume V_0 taken up by a single particle is $V_0 = \frac{4}{3}\pi\left(\frac{d}{2}\right)^2$, where d is the diameter of every particle. The solid volume fraction is defined as $\phi = \rho_\# V_0$. In this simulation, the particle diameter is used as the unit length.

Deformation of the system causes particles to move. Deformation disrupts mechanically stable positions, which causes a change in the internal stresses that further induces particle movement. Random thermal energy also causes particles to move. In this investigation, in order that I can focus on the effect of the imposed strain, thermal energy is drained from the system before applying strain. This makes $k_B T$ very small with respect to the depth of the attractive well ϵ. This is accomplished through a process called damping.

Damping is accomplished by letting the system evolve following this equation of motion:

$$m\frac{d^2\vec{r}_i}{dt^2} = -\xi\frac{d\vec{r}_i}{dt} - \vec{\nabla}_{r_i}U$$

where m is the particle mass and ξ is a drag coefficient. As the system iterates through several damping steps, kinetic energy is dissipated through the drag term $\left(\xi\frac{d\vec{r}_i}{dt}\right)$. This simulates a solvent permeating the gel network, which damps the thermal vibrations of the gel particles without returning any of the energy to the gel particles.

[c] The u_2 term, however, effects the physical meaning of a bond in the simulation. The distance r^* at which u_2 reaches a minimum is the stable distance which bonds describe.

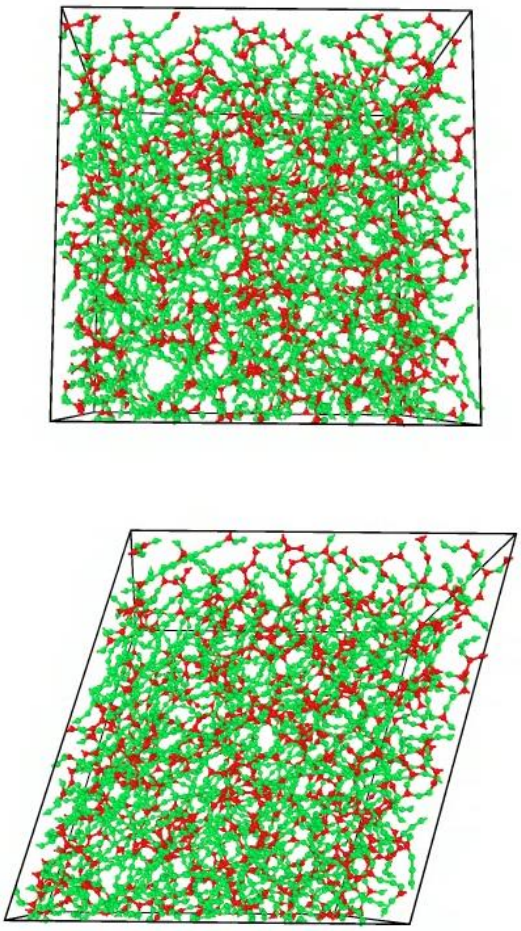

Figure 10. *Two snapshots of the simulation box under shear. This comes from a system in which $\bar{\theta} = 70°$. The image on the left is the simulation box before shearing begins; the image on the right is after a significant amount of shear, shortly before an accumulated shear of 50% has been applied. Shearing of the xy faces (top and bottom lines) renders a parallelogram. The face visible from this vantage point is the yz plane. Using Lees-Edwards Boundary Conditions, there are copies of the simulation box bordering the simulation box above and to the sides. The miniature spheres represent gel particles, and the string-like structures connecting them represent bonds. Particles in green have a coordination number of 2 and particles in red have a coordination number of 3. A general bond alignment trend, that roughly parallel to the long diagonal of the parallelogram in the right-hand image, is visible.*

The system is damped until $\frac{k_B T}{\epsilon} < 10^{-10}$, at which point the kinetic energy is negligible. This is usually accomplished within 5×10^6 steps of $\Delta t = 5 \times 10^{-3}\ \tau^*$, where the unit time $\tau^* = \sqrt{\frac{md^2}{\epsilon}}$. m and d are the mass and diameter of the particle, respectively. $\bar{\theta}$=65° for this step in all tests in order to make initial formation of the gel consistent.

The simulation box is initially a cube (Fig. 10). As strain is applied in the *xy* plane, the *xy* dimensions of the space adjust to accommodate the strain. The top edge of the cube appears to be pulled in the *x* direction, analogous to how a single block of material would bend if a sliding plate along the top were generating shear. I use periodic boundaries with Lees-Edwards boundary conditions (see Fig. 11) that allows us to maintain the deformation.[34]

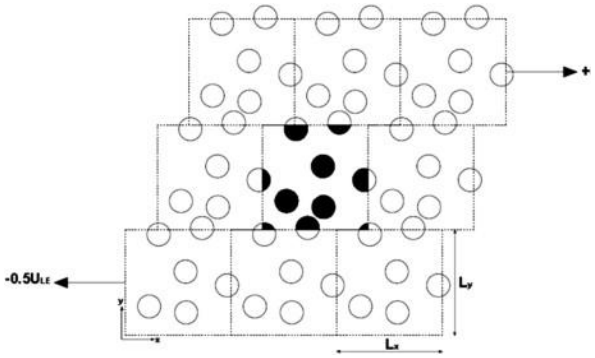

Figure 11. *Lees-Edwards boundary conditions. The simulation box is surrounded by copies of itself on all sides. The features disappearing through one face of the simulation box reappears in the opposite face. The simulation boxes bordering on the top and bottom are staggered. Shear strain is applied by moving the boxes bordering the top of the simulation box in the +x direction and the moving the boxes bordering the bottom in the –x direction by an equivalent amount. This drags along the top and bottom faces of the box in opposite directions, rendering shear strain within the box.*

B. Varying the stiffness of the gel branches

After the initial damping, the value of $\bar{\theta}$ is changed to the new test value, which range from 55° to 67° in this investigation. The system is again damped until $\frac{k_B T}{\epsilon} < 10^{-10}$ for the same number of steps, but at the new test value of $\bar{\theta}$. Such protocol is necessary to make sure I start the mechanical tests in similar conditions for all gels studied.

After the two intervals of damping, the system is deformed in two repeating steps, keeping $\bar{\theta}$ at its test value. First, a simple shear strain is applied in the *xy* plane, defined as $\Gamma_{\Delta\gamma}$:

$$\boldsymbol{r'_i} = \Gamma_{\Delta\gamma}\boldsymbol{r_i} = \begin{pmatrix} 1 & \Delta\gamma & 0 \\ 0 & 1 & 0 \\ 0 & 0 & 1 \end{pmatrix}\boldsymbol{r_i}$$

Second, the stresses accumulated during this deformation step are relaxed:

$$\boldsymbol{r''_i} = \mathcal{T}_{\Delta t}\boldsymbol{r'_i}$$

where $\mathcal{T}_{\Delta t}$ is the time evolution operator for damped dynamics over a time interval Δt. After n cycles (each made of the 2 steps), the accumulated strain is $n\Delta\gamma$ and the final position of a given particle is $\left(\mathcal{T}_{\Delta t}\Gamma_{\Delta\gamma}\right)^n \boldsymbol{r_{i,0}}$, where $\boldsymbol{r_{i,0}}$ is the position of the particle at the end of the damping intervals *a* and *b*. The magnitude of deformation steps ($\Delta\gamma$) must be small compared to the particle size. From this procedure I can define a strain rate $\dot{\gamma} = \frac{\Delta\gamma}{\Delta t}$. The rate can be adjusted by varying Δt. In these simulations, $\Delta\gamma$ = 0.01L, where L is the length of the simulation box.

Results & Discussion

As previously mentioned, the differential modulus K is calculated halfway between each coordinate pair of shear strain and shear stress (Fig. 12). The value of the modulus at each stress and strain halfway point is the slope between the two adjacent coordinates. The stress (σ) and strain (γ) values used alongside the modulus are also halfway between the original coordinates, calculated as averages of the two coordinates.

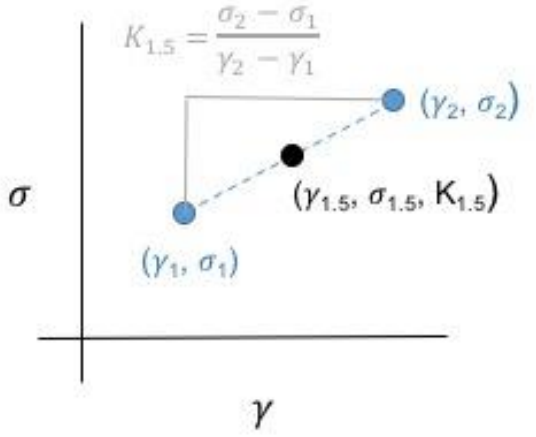

Figure 12. The shear modulus K is calculated as the slope between two consecutive (γ, σ) coordinates on a load curve. The modulus value is treated as belonging to a point halfway between the two points. The γ and σ of this point halfway between the two points on the initial load curve are calculated as the average of the γ and σ of the initial two consecutive (γ, σ) coordinates.

I use three graphs to depict the mechanical response of each gel network: (a) the load curve, and the differential modulus (K) as (b) a function of stress and (c) as a function of strain (Fig. 13). For simplicity, I use K(σ) to describe the graph of the differential modulus (K) as a function of shear stress (σ_{xy}), and K(γ) to describe the graph of the differential modulus (K) as a function of shear strain (γ_{xy}).

As expected, the load curve begins as a linear relationship between stress and strain but begins to increase exponentially after some intermediate level of accumulated strain, γ_c (Fig. 3, Fig. 13c). However, the distinction between the two regions is ambiguous, especially in the context of the load curve alone. In fact, the two regions may even overlap since both the elastic

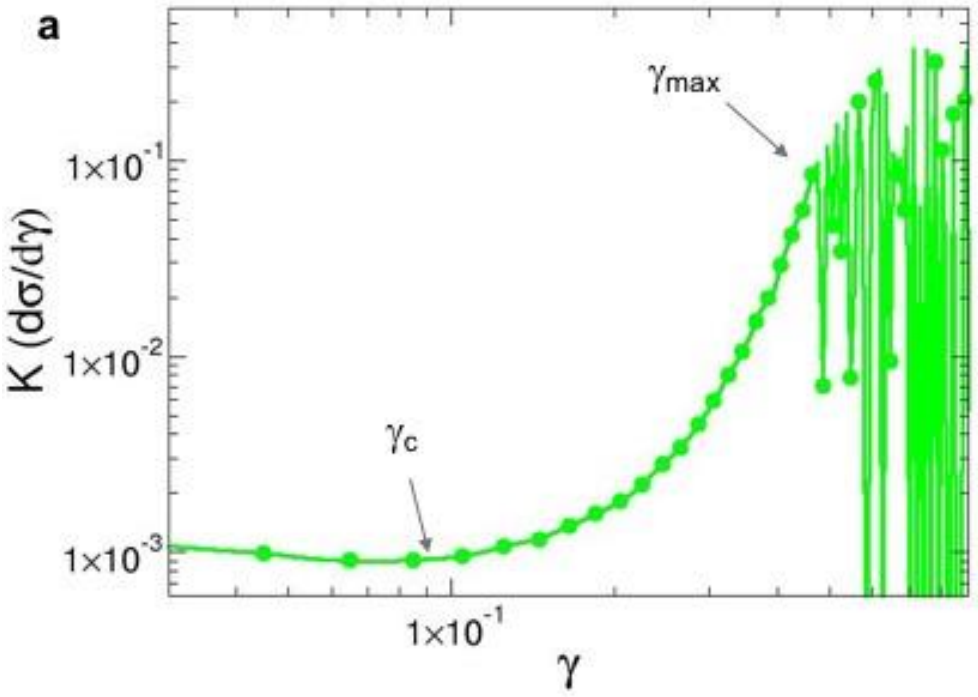

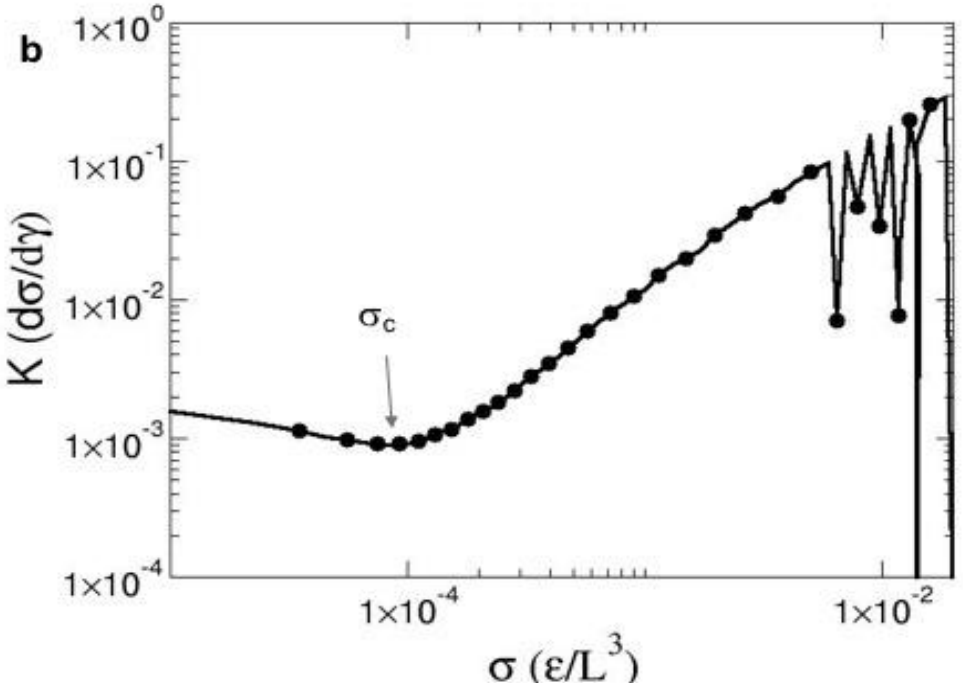

responses (linear) and stiffening responses (exponential) may exist concurrently in different regions of the gel. This overlap would manifest itself in the load curve as an ambiguous region which is too large to be linear but also is not large enough to achieve the exponential growth rate that is apparent at higher strains. Even without this region, discerning such a transition point from the load curve is impractical, as the initial exponential increase is so slightly higher than a linear increase that it would appear linear to both human eye and best fit algorithms. I use, instead, the graphs of the differential modulus to determine γ_c and its resulting stress value, σ_c. Since K is the first derivative of σ with respect to γ, $K(\gamma)$ is essentially a plot of the load curve's slope (Fig 13a). As such, a drastic increase in $K(\gamma)$ shows γ_c more clearly than the load curve. Curiously, there is often a minimum in $K(\gamma)$ before it makes such a drastic increase (Fig. 13a). I use this minimum, when present, as γ_c. Similarly, the increase in $K(\sigma)$ contains a minimum before its value sharply increases, which I use as σ_c. This minimum exists because σ increases

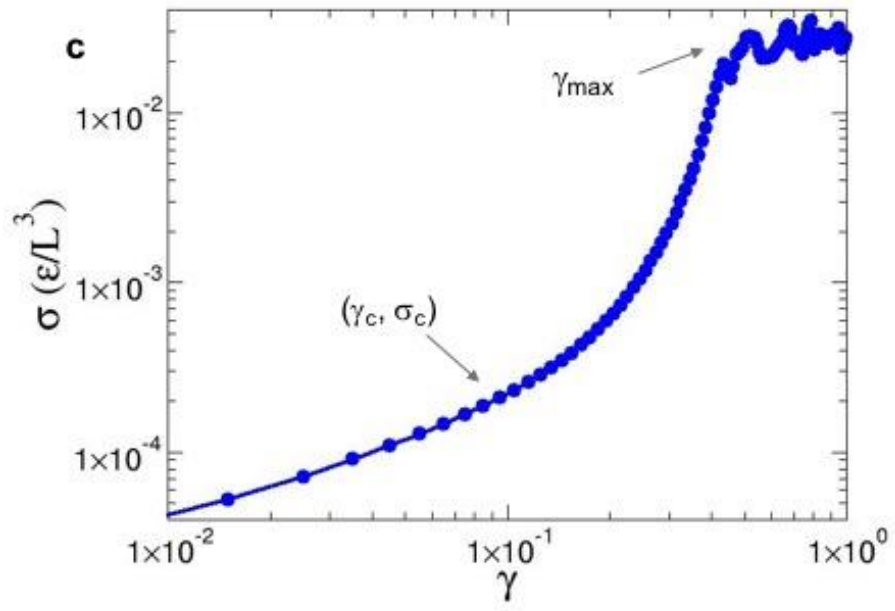

Figure 13. *Average plot of load curve, K(γ), and K(σ) for $\bar{\theta} = 70°$. **a)** Plot of the differential modulus (K) with respect to strain (γ). γ_c is measured as the strain at which K reaches its first minimum. γ_{max} is measured as the strain at which K reaches its first local maximum before the function becomes erratic. **b)** Plot of the differential modulus (K) with respect to strain (σ). σ_c is measured as the stress value at which K reaches its first minimum. **c)** Load curve. γ_c and σ_c occur where load curve transitions from linear to nonlinear, though this point is difficult to interpret. γ_{max} is measured as the strain at which the curve ceases to increase smoothly.*

monotonically with γ in the load curve. Values of γ_c extracted in this manner correspond to value of σ_c on the load curve.

All gels in a single macrostate set have the same number density of ϕ=7.5%, 4000 member particles, and the same $\bar{\theta}$ value. A macrostate set was analyzed for each value of $\bar{\theta}$ at 1° intervals for $55° \leq \bar{\theta} \leq 76°$. The only difference between the four gels within a particular macrostate set is the length of time during sample preparation at which the system energy ($\frac{k_B T}{\epsilon}$) is held at 1. The high temperature provides extreme thermal energy to randomize the initial positions of the particles, so varying this length of time should render four unique gels. To be consistent, the same four prepared gels (labeled *a*, *b*, *c*, and *d*) were used at every value of $\bar{\theta}$.[d] Averaging the load curves of the four gels in each macrostate set combines the separate but consistent trends for each family of gels into an equally consistent average trend. However, it is curious that one prepared state, *d*, has a consistently higher γ_{max} than the other states. The attempt to randomize prepared gels has somehow created prepared gels with a clear hierarchy of these particular properties, although slight in their differences. Since prepared states *a-d* have equivalent macrostates, I suppose that particular arrangements of particles at the end of the heating interval by chance happen to be mechanically superior to other particular arrangements. The quality that makes an arrangement so mechanically superior can at this point only be guessed.

Identifying γ_{max} was incredibly challenging, and not easily done using the load curve alone. The load curve tended to remain continuous, but often contained multiple local minima after γ_c which could be interpreted as γ_{max}. Typically, γ_{max} would be the local minimum that occurs at the lowest value of strain after γ_c. However, comparisons between different load curves showed

[d] Recall that the initial preparation process is done at $\bar{\theta} = 65°$ for all samples, regardless of the $\bar{\theta}$ value being tested (Methods -> Model -> Preparation Protocol).

that this point varied greatly even for different simulated gels with the same value of $\bar{\theta}$. Gels in the same macrostate set had a significant spread of values γ_{max}, but gels with the same initial prepared configuration changed with $\bar{\theta}$ in a way that was consistent between each family of gels, just as with γ_c and σ_c.

Using the average of each macrostate set load curve should take care of this problem, though in the case of γ_{max} the averaged load curve makes the story more complicated. For $\bar{\theta} = 65°$, the average load curve for our macrostate set shows a few key differences with the load curve of a single gel that was much larger, where $N \approx 20{,}000$. The larger gel's curve remains smooth up to higher levels of strain and thus has a significantly higher γ_{max} value based off the load curve alone. Additionally, the portion of the curve common to both graphs is significantly smoother for the large gel's curve. This shows that many of the fluctuations in the load curve at high accumulated strain is a result of irregularities in the system rather than of an intrinsic limit of the gel.

If the only difference between the average load curve and the large system load curve is the number of particles and bonds sampled, one can expect that a smoother curve results because the stress response is more easily normalized among a greater population of particles. This idea is also apparent in the difference between the average load curve and each of the individual load curves in a macrostate set. The γ_{max} value of the average load curve is not the average of the γ_{max} in each of the individual load curves, but rather is greater in most cases. The average load curve, which samples four times as many particles as an individual load curve, is smooth at values of γ that see fluctuation in the individual load curves due to system-specific irregularities. In fact, both the average load curves and the large system curve still seem to increase after they begin fluctuating. One might even be able to draw a smooth line through the fluctuating path by averaging the values. This shows that chasing a perfect curve, completely devoid of these fluctuations arising from system-specific irregularities, would require simulating massive systems far beyond the available computing power and the available time of the undergraduate performing this investigation.

As with γ_c, my alternative method for determining a specific γ value is to look at $K(\gamma)$. I determine γ_c to be the first local maximum on $K(\gamma)$ (Fig. 13c). This first local maximum seems to be a result of irregularities, as it always precedes a precipitous drop in K to a negative value, which theoretically should not exist. However, the irregularities are not system-specific since this maximum precedes such a precipitous at every value of $\bar{\theta}$, and the feature is consistent across all individual $K(\gamma)$ curves in the macrostate set.

Viewed together, the trends of γ_{max} and γ_c as a function of $\bar{\theta}$ show that the nonlinear regime becomes smaller with increased bending rigidity. That is, after the system reaches γ_c, a higher bending rigidity means that less additional strain is needed to bring the gel to its yield point (Fig. 14). γ_{max} decreases slowly with $\bar{\theta}$ at first, but becomes more rapid as $\bar{\theta}$ increases. I see that γ_{max} begins to plummet near $\bar{\theta} = 76°$, suggesting that the gel would break at negligibly small levels of strain at higher values of $\bar{\theta}$. Fittingly, simulations at values of $\bar{\theta}$ higher than 76° produces load curves that are not meaningful with respect to the rest of the simulations: values of stress are orders of magnitude lower and features such as the yield point are not even present for $\bar{\theta} > 78°$. Previous research with this model has shown that γ_{max} decreases with increasing $\bar{\theta}$. γ_c drops steadily as $\bar{\theta}$ increases from 60° to 66°, but remains essentially constant for $\bar{\theta} > 66°$.

Recall that a shrinking of the nonlinear regime also occurs with increased density of the sample. I can explain the shrinking nonlinear regime due to bending rigidity using the same

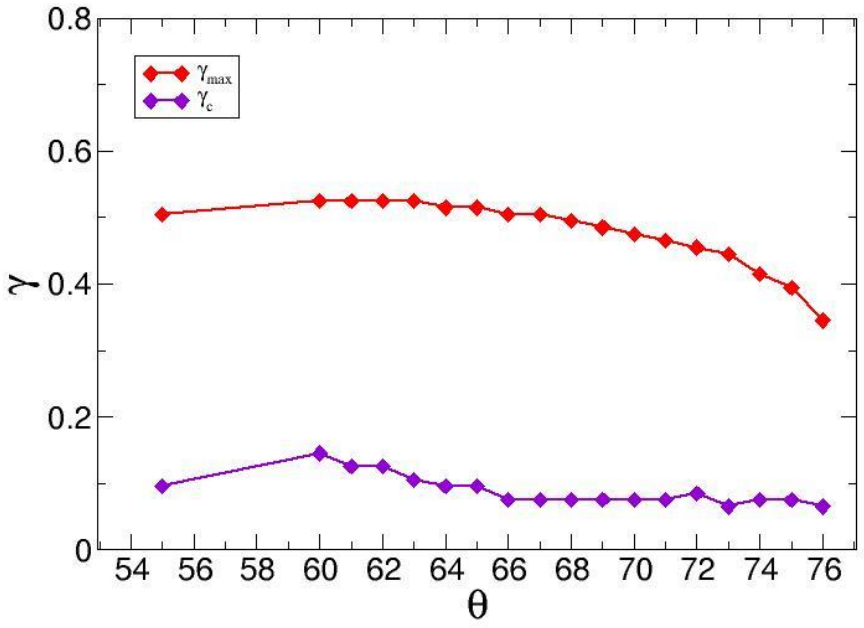

Figure 14. *Change in γ_{max} and γ_b as a function of $\bar{\theta}$. γ_b is the level of accumulated strain at which the coordination number distribution begins to change from its initial distribution. This is the point at which rate of bond destruction surpasses rate of bond formation. γ_{max} is the yield strain, as calculated from the K(γ) curve. Both values were measured with at every degree value for $60° \leq \bar{\theta} \leq 76°$ and also for $\bar{\theta} = 55°$.*

mechanism. With denser networks, the stress builds up in the stretching modes because the increased connectivity (i.e. more nodes) prevents the gel branches from rearranging to accommodate the deformation. Similarly, I can picture that increased bending rigidity also restricts the gel network's ability to rearrange to accommodate deformation. The potential energy associated with a filament joint at a particular angle $\theta > 90°$ becomes larger with a higher $\bar{\theta}$. As a result, filament joints have a harder time closing more tightly. For the network structure to rearrange to accommodate deformation, some joints must close tighter, but with this restriction on bending, the network is not able to rearrange as easily. Bending modes may thus favor deformation at lower bending rigidity but resist deformation at higher bending rigidity.

The way in which the nonlinear regime shrinks with increased $\bar{\theta}$ is different than with increased density. With density, γ_{max} decreases in the manner of a negative exponent (dropping quickly at low strains then leveling out at high strains) while with bending rigidity, γ_{max} drops in the manner of a positive exponent (dropping slowly if at all for low strains before taking a sudden, deep dive at high strains) (Fig. 14, Fig. 5). Increasing rigidity does not restrict network motion until very high values of $\bar{\theta}$, while increasing density seems to do so at all values. I believe increased $\bar{\theta}$ has a delayed effect because it affects the mechanics on a more fundamental, more microscopic level than density. While the ratio of nodes to chain links varies with density, filament joints across varying densities are subject to the same energy restrictions. The energy landscape for any given filament joint changes completely across varying bending rigidity, however.

Consider a system with a low $\bar{\theta}$, say $\bar{\theta} = 55°$. The bond angles, which are largely if not completely greater than $90°$, are too far removed from the repulsive power of the u_3 maximizing angle $\bar{\theta} = 55°$ to be significantly affected. A typical joint might need only bend across a certain range of angles to adequately react to deformation. Call this range of angles the necessary angular domain. None of these angles would require more energy to achieve than the internal stresses can

provide. As $\bar{\theta}$ inches closer to the lower bound of the necessary angular domain, however, the smaller angles in the necessary angular domain cannot be achieved with the available stresses, since the u_3 term for a joint at this angle is increasing. As a result, only exceptionally strong local stresses can press the joint into this part of the necessary angular domain. Other joints may need to pass only through the higher angles in the necessary angular domain to react to deformation, and these rearrangements occur as easily as before. As $\bar{\theta}$ inches yet closer to the necessary angular domain, all angles in the domain are affected. Before, only joints that wished to pass through the lower values in the necessary angular domain to achieve a relaxed structure were affected. Now, even the joints that do not wish to change are affected, pushed by the u_3 term to angle values at the upper end of and potentially higher than the necessary angular domain. I propose that this transition is the causes the bending modes to transition from supporting to resisting the deformation. Once all angle values within the necessary angular domain are under significant pressure from the u_3 term, only exceptionally strong local stresses can push angles through the domain. Any further increase in $\bar{\theta}$ quickly shrinks the nonlinear regime, as fewer strong local stresses remain exceptional enough to fight the u_3 term. When the joints are no longer able to bend freely, the stretching modes take the brunt of the deformation stresses.

There could be an entirely different reason for this rapid decrease in γ_{max}, though these results alone cannot offer any substantial alternative explanations. Additionally, this investigation's definition of γ_{max} may be different than the definition in the study that quantified the effects of density, meaning that the differences are simply that of measurement technique. It would still be interesting, though, if the trend in γ_{max} is the same in both cases. γ_c drops in a much more similar manner in both plots, swiftly at first but essentially unchanging for further increases in density or bending rigidity.

In addition to the size, the form of the nonlinear regime offers further insight. As discussed before, the nonlinear regime can be described by the exponent α. Despite the straightforward definition $K = A\sigma^{\alpha}$ that relates α neatly to K, deriving α from K(σ) is a challenge. The difficulty lies almost entirely in determining the bounds of the stiffening regime which α describes. Once the bounds of the stiffening regime are defined, graphing software[e] can easily calculate a best fit line of the form $y = a_0 x^{a_1}$ over the selected region, from which the a_1 term is understood to be α.

Since $K = A\sigma^{\alpha}$, a simple method to determine the range of the non-linear regime described by α is to generate functions of various σ^x where x covers the expected range of α from 1 to 2. K can then be normalized separately by each of these functions, giving $K/\sigma^x = A\sigma^{\alpha}/\sigma^x$. This will render a constant function of A when $\alpha = x$. I attempted to locate the bounds of the non-linear regime by using this approach on a few K(σ) plots. The results, however, were ambiguous. No K/σ^x was a constant function throughout the entirety of the stiffening regime. Borrowing pieces from two of the K/σ^x lines can produce a flat line for most of the non-linear regime with disruptions only before, after, and between the two pieces. Such a plain change in value of α indicates that there are two distinct stiffening regimes. The possibility of multiple stiffening regimes matches observations made on a similar system using a different model, which shows two separate stiffening regimes, each having a distinct value of α.[7,27] Along the low stress stiffening regime (i.e. that which directly follows the linear regime), just as along the linear regime, bending modes are dominant; along the high stress stiffening regime (i.e. that which occurs immediately before breaking), stretching modes are dominant.[27] This suggests that the boundary between these

[e] I used various iterations of Grace, XMGrace for Linux and QTGrace for MacOS.

non-linear regimes occurs at the stress at which the strength of stretching modes surpasses those of the bending modes.

Because of this insight, the nonlinear portion of K(σ) was split into two intervals for fitting the curve. Indeed, a fit of the full nonlinear interval renders a plot that, though fairly similar to the curve, is inconsistent with significant portions of the curve. Fitting two intervals separately renders fits that are more exact (Fig. 15). While there are portions of the nonlinear regime at high σ and at low σ that clearly fit in the high stress and low stress, respectively, portions near the middle of the nonlinear regime were difficult to place. Many of the regimes are separated by a small interval rather than having an immediate transition between the two. This interval is marked often by a fluctuation in the function, but the fluctuation may be independent of the transition since similar fluctuations exist in the in the dead middle of clearly defined regions elsewhere. I determine the regions by drawing a line that appears to be

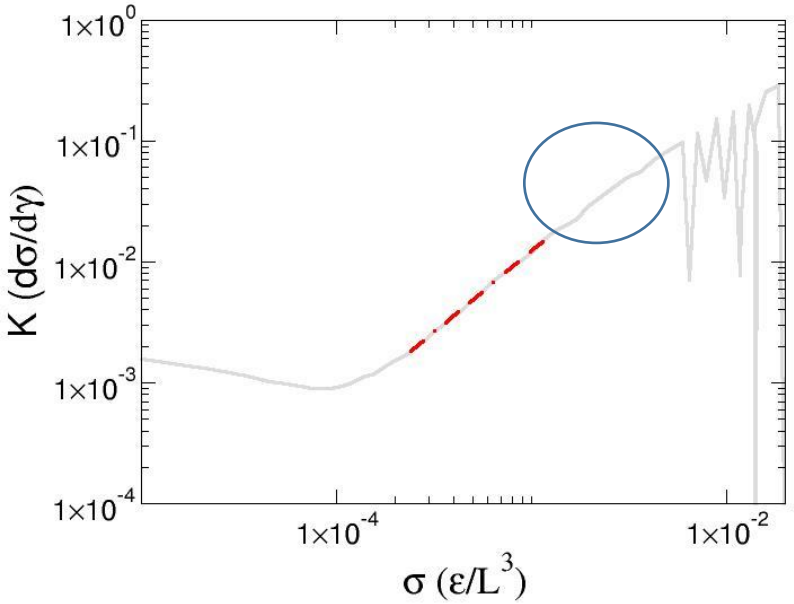

Figure 15. *A fit of the nonlinear regime for $\bar{\theta} = 70°$. The dashed line shows the range and form of the best fit function for the low strain nonlinear regime. Portions most suitable for fitting appear as a straight line on these plots, and the longest stretch of plot that appears to run along such a line is included in the fit region. A high strain nonlinear regime (circled) also exists for most averaged K(σ) curves. This high strain regime becomes small for $\bar{\theta} = 75°$, about ½ or less than ½ the length of the high strain regime pictured here.*

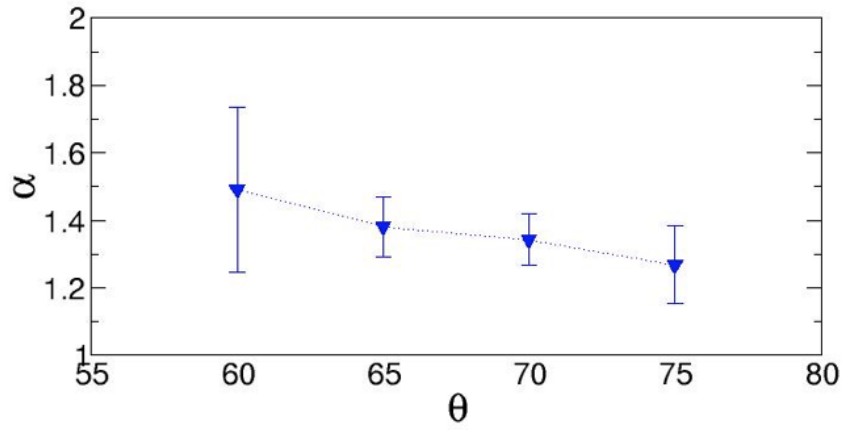

Figure 16*. α for the low strain linear regime as a function of $\bar{\theta}$. Data points are the α fit of the averaged K(σ) curve of the 4 systems tested at each value of $\bar{\theta}$. Error bars are the standard deviation of the α values of the 4 individual K(σ) curves from the average.*

parallel with a large portion of K(σ), marking the two edges of the region where the function ceases to be parallel with the line.

The α values of the full nonlinear regime and the high strain nonlinear regime do not show any consistent trends. Interestingly, I find that the upper region shrinks as to become nearly indistinguishable at high values of $\bar{\theta}$. This high stress nonlinear regime has been tagged in previous simulations as being dominated by stretching modes.[27] The disappearance of this regime at high $\bar{\theta}$ is surprising, then, since I would initially assume that increased bending rigidity suppresses the action of bending modes and thus leaves the bulk of the response to the stretching modes. Although the bending modes are not allowing motion, however, they may still be resisting the deformation. In fact, increasing $\bar{\theta}$ makes the joints less likely to move and therefore more stress will likely collect in the attempt to move the stiffening joints. Stiffer networks can, after all, bear more stress, so it makes sense that the stiffer mode within the network is taking on all the stress.

Analysis of the low stress nonlinear regime, by contrast, shows a clear dependence of α on $\bar{\theta}$: α decreases monotonically with an increase in $\bar{\theta}$ (Fig. 16). However, this change is too slight to account for the differences in α between the featured model and the other popular simulation model, or between actin and collagen. As mentioned, the other model shows α values ranging from ½ to 1. The apparent trend in Fig. 16 cannot even approach 1.2, let alone drop below 1 due to the increased bending rigidity. One might hope that high enough values of $\bar{\theta}$ would render comparable α values, as I might expect that α would steadily decrease infinitely as $\bar{\theta}$ increases. The mechanical response of the system begins to radically deviate from realistic load curves after $\bar{\theta} = 76°$, though. As a result, the relationship between α and $\bar{\theta}$ loses all significance shortly after $\bar{\theta} = 75°$. The bending rigidity, at least as it is defined in the featured model, is not a contributing factor to the difference in the nonlinear regime between the two simulation models or between collagen and actin.

Interestingly, the decrease in α thanks to increased bending rigidity is not as extreme as the decrease thanks to increased density. α is shown to be 3/2 for densities of 5% and 7.5% but decreasing to 1 at 10% and to a much lower value at 15%.[19] Like with bending rigidity, the decrease in α corresponds to the decrease in the length of the nonlinear regime.

Since $\mathbb{C}_3$ nodes are known to bear strain, there is some significance in the level of accumulated strain at which $\mathbb{C}_3$ bonds began to break. This level of strain, γ_b was measured as the level of strain at which the coordination distribution in a given sample begins to deviate from its initial value. I measure it this way because data shows that, at this point, $\mathbb{C}_3$ particles convert to $\mathbb{C}_2$ particles, which mean that bonds are breaking. The values of $\mathbb{C}_2$ and $\mathbb{C}_3$ remain constant at their initial values for a significant amount of time, then change at the same time, and $\mathbb{C}_3$ always decreases by the exact same amount that $\mathbb{C}_2$ increases.

Through the values of $\bar{\theta}$ tested, I find an unmistakable correlation between γ_b and γ_{max}, with a notable exception in the domain $64° \leq \bar{\theta} \leq 70°$ (Fig. 14). In this domain, there is a large jump in γ_b which carries it away from any definite correspondence with γ_{max}. This confirms that yield strain γ_{max} occurs when the number of bonds breaking exceeds the number being formed. Even one or two bonds breaking trigger the failing of the entire gel because few bonds have been collecting a majority of the stresses resulting from the deformation.

Conclusion

I confirm that, with an increase in bending rigidity embodied in an altered $\bar{\theta}$, the nonlinear regime rapidly shortens. I can attribute this trend to the decreased ability of the network to rearrange itself to accommodate deformation, similarly to the effect of increased network density. In contrast to the effect of density, the effect of bending rigidity is slower to appear but the effect accelerates rapidly once it is manifested. I attribute the slow onset to the insignificant effect of the u_3 term when $\bar{\theta}$ is far from the necessary angular domain. The stiffening rate α decreases with increasing $\bar{\theta}$. This change is not drastic enough, however, to explain the differences between simulation models or between measurements for actin and collagen using the other popular model. A distinct high stress nonlinear regime, whose dependence on $\bar{\theta}$ and significance are not yet known, exists at higher values of γ. γ_b is intrinsically linked to γ_{max}, as expected.

A further investigation of the necessary angular domain is in order. In particular, it is important to understanding the minimum and maximum limits of the necessary angular domain, as well as the distance at which $\bar{\theta}$ begins to significantly affect the accessibility of angles in the

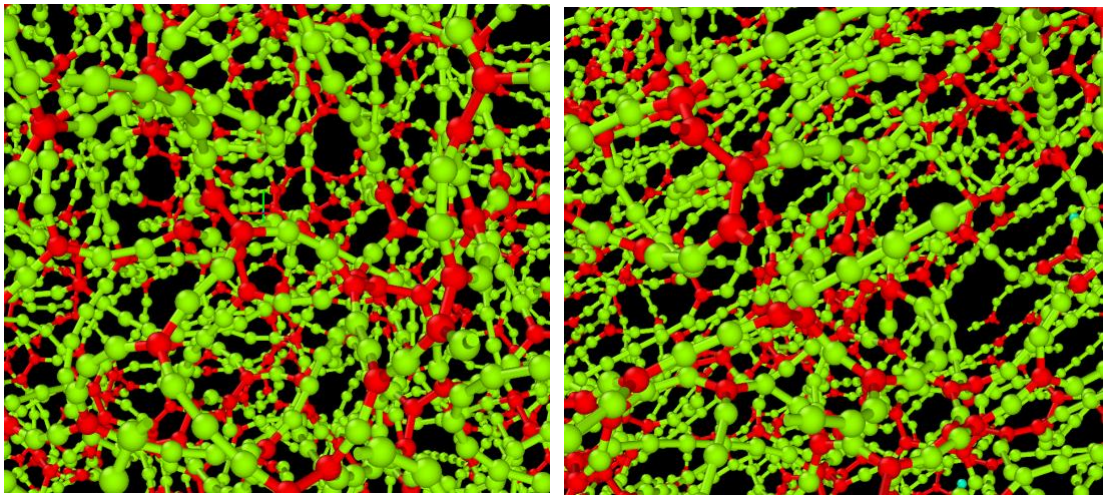

Figure 17. *Snapshots of a gel network before (left) and after (right) a full simulation box length (L) of shear strain. The chains within the network (green) are significantly aligned along the direction of maximum extension after the deformation, while their direction are more or less randomized beforehand.*

domain. In order for the bending rigidity to be useful as a control parameter for gel mechanical response, it must be known how various levels of bending rigidity will affect each gel with its particular microscopic preferences. This investigation hints that the preferred angles of bonds in a particular gel are one such important microscopic preference.

The main mechanism presented to explain the changing form of the nonlinear regime deals primarily with the ability of the network to readjust in response to deformation. The order parameter is an ideal quantitative measure of how well the network readjusts. The order parameter defines how well-aligned (i.e. how parallel) bonds are in a system at a particular time. The tensor order parameter is defined as:

$$Q_{\alpha\beta} = \langle u_\alpha u_\beta - \frac{1}{3}\delta_{\alpha\beta} \rangle$$

where u_α and u_β are unit vectors representing the direction of any two bonds in the system.[35] $Q_{\alpha\beta}$ is 0 when bond orientations are perfectly random and becomes nonzero as bonds align.

In an ideal response to deformation, filaments in the system would align in the direction of principal tension. Qualitatively, bonds appear to align strongly in the direction of strain as strain accumulates (Fig. 17). Therefore, a gel network that is able to readjust to accommodate deformation will be expected to exhibit easier alignment as strain accumulates. Systems with higher density, which I describe to have difficulty adjusting to deformation, show poor alignment.[19] I hypothesize that increased bending rigidity will have a similar effect, though hope that such a decrease in alignment tendencies might show a nuanced pattern of weaker alignment with more bending rigidity that would shed more light on why increased density and increased bending rigidity have differently patterned effects.

Acknowledgments

I would like to thank, first and foremost, Professor Del Gado for an extraordinary commitment of time and patience in helping me conduct this research and compose this report. The author missed many internal deadlines imposed by both Professor Del Gado and himself, yet she remained fully engaged with prompt, detailed feedback even in spite of her own tight professional and personal schedule, coordinated across 3 time zones and 2 continents. Thank you for working through my often overly wordy writing time after time, often peppered with colloquial words that confused the scientific meaning. Discussions on the subject matter and the texts you lent me have been invaluable references.

I would like to thank Minsaspi Bantawa for frequent and expert assistance in the computational arts, especially regarding the featured simulation model. Processes I could not have performed without his presence include but are not limited to: understanding the potential terms in the model, editing LAMMPS scripts to retrieve custom information from the simulation, crafting Python and C++ scripts to extract and process new kinds of data, and using some of the somewhat hidden plotting features of XMGrace. In short, without his presence, I would not have accomplished much more than creating a dent in the wall by frequent banging of my head against it. Mehdi Bouzid was irreplaceable in getting me started down this path, taking a great deal of time to teach me the mechanics of the simulation model, the physics behind it, and the best practices for computational and data-extracting processes.

I would like to thank Professors Mak Paranjape and Christopher Cothran for offering helpful feedback on the presentation of the material, especially given the potentially exorbitant length of this thesis report. I could not go without mentioning Professor Rhonda Dzakpasu's

attention in organizing group sessions to guide our research and report-writing processes. Thank you also to the many fellow undergraduates who accompanied me on this journey for their support and report writing feedback, including but not limited to Alex Morales-Sanz, Caitie Beattie, Isabel Binamira, Max Waxman, Benjamin Stein-Lubrano, Christian Stiker, Thomas Kiely, and Will Thacher. I would like to credit the creators of the citation management tool Mendeley for saving me dozens of hours of what would have been correcting reference listings that were mismatched with relevant points in the text and neglecting important information in the citation listing. Thank you lastly to my parents and to Hannah Funk for emotional support through stressful weekends and late nights in the lab.

Figure Sources

Figure 1 [36], Figure 3 [33], Figure 4 [28], Figure 5 [19]

References

1. Larson, R. G. Introduction to Complex Fluids. in *The Structure and Rheology of Complex Fluids* 3–60 (Oxford Univ. Press, 1999).
2. Doi, M. What is soft matter? in *Soft Matter Physics* 1–7 (Oxford Univ. Press, 2013).
3. Ladd, M. Classical solids. in *Bonding, Structure and Solid State Chemistry* 285–86 (Oxford Univ. Press, 2016).
4. Gibaud, T., Zaccone, A., Del Gado, E., Trappe, V. & Schurtenberger, P. Unexpected Decoupling of Stretching and Bending Modes in Protein Gels. *Phys. Rev. Lett.* **110,** 58303 (2013).
5. Maitra, J. & Shukla, V. *Cross-linking in hydrogels - a review*. *Am J Polym Sci* **4,** (2014).
6. Doi, M. Elastic soft matter. in *Soft Matter Physics* 28–50 (Oxford Univ. Press, 2013).
7. Broedersz, C. P. & MacKintosh, F. C. Molecular motors stiffen non-affine semiflexible polymer networks. *Soft Matter* **7,** 3186–3191 (2011).
8. Conti, E. & MacKintosh, F. C. Cross-Linked Networks of Stiff Filaments Exhibit Negative Normal Stress. *Phys. Rev. Lett.* **102,** 88102 (2009).
9. Davidson, M. W. Animal Cell Structure. *Molecular Expressions* (2015). Available at: https://micro.magnet.fsu.edu/cells/animalcell.html. (Accessed: 3rd December 2017)
10. Microtubules and Filaments. *Scitable* (2014). Available at: https://www.nature.com/scitable/topicpage/microtubules-and-filaments-14052932. (Accessed: 3rd December 2017)
11. Masoero, E., Del Gado, E., Pellenq, R. J.-M., Ulm, F.-J. & Yip, S. Nanostructure and Nanomechanics of Cement: Polydisperse Colloidal Packing. *Phys. Rev. Lett.* **109,** 155503 (2012).
12. Banerjee, S. & Bhattacharya, S. Food Gels: Gelling Process and New Applications. *Crit. Rev. Food Sci. Nutr.* **52,** 334–346 (2012).
13. Allen, P. W. & Bristow, G. M. The gel phase in natural rubber. *J. Appl. Polym. Sci.* **7,** 603–615 (1963).
14. Sottos, N. R. & Moore, J. S. Spot-on healing. *Nature* **472,** 299 (2011).
15. Cordier, P., Tournilhac, F., Soulié-Ziakovic, C. & Leibler, L. Self-healing and thermoreversible rubber from supramolecular assembly. *Nature* **451,** 977 (2008).
16. Storm, C., Pastore, J. J., MacKintosh, F. C., Lubensky, T. C. & Janmey, P. A. Nonlinear elasticity in biological gels. *Nature* **435,** 191 (2005).
17. Gaharwar, A. K. *et al.* Shear-Thinning Nanocomposite Hydrogels for the Treatment of Hemorrhage. *ACS Nano* **8,** 9833–9842 (2014).
18. Yan, C. *et al.* Injectable solid hydrogel: mechanism of shear-thinning and immediate recovery of injectable [small beta]-hairpin peptide hydrogels. *Soft Matter* **6,** 5143–5156 (2010).
19. Bouzid, M. & Del Gado, E. Network Topology in Soft Gels: Hardening and Softening Materials. *Langmuir* (2017). doi:10.1021/acs.langmuir.7b02944
20. Wen, Q., Basu, A., Janmey, P. A. & Yodh, A. G. Non-affine deformations in polymer hydrogels. *Soft Matter* **8,** 8039–8049 (2012).

21. Lieleg, O., Kayser, J., Brambilla, G., Cipelletti, L. & Bausch, A. R. Slow dynamics and internal stress relaxation in bundled cytoskeletal networks. *Nat. Mater.* **10,** 236 (2011).
22. Sadati, M., Nourhani, A., Fredberg, J. & Taheri Qazvini, N. *Glass-like dynamics in the cell and in cellular collectives*. *Wiley interdisciplinary reviews. Systems biology and medicine* **6,** (2014).
23. Kurniawan, N. A., Enemark, S. & Rajagopalan, R. The role of structure in the nonlinear mechanics of cross-linked semiflexible polymer networks. *J. Chem. Phys.* **136,** 65101 (2012).
24. Sharma, A. *et al.* Strain-controlled criticality governs the nonlinear mechanics of fibre networks. *Nat. Phys.* **12,** 584 (2016).
25. Landau, L. D. & Lifshitz, E. M. Fundamental Equations. in *Theory of Elasticity* 1–38 (Elsevier, 1986).
26. Doi, M. Flow and deformation of soft matter. in *Soft Matter Physics* 165–96 (Oxford Univ. Press, 2013).
27. Licup, A. J. *et al.* Stress controls the mechanics of collagen networks. (2015). doi:10.1073/pnas.1504258112
28. Colombo, J. & Del Gado, E. Stress localization, stiffening, and yielding in a model colloidal gel. *J. Rheol. (N. Y. N. Y).* **58,** 1089–1116 (2014).
29. Broedersz, C. P. & MacKintosh, F. C. Modeling semiflexible polymer networks. *Rev. Mod. Phys.* **86,** 995–1036 (2014).
30. Broedersz, C. P., Sheinman, M. & MacKintosh, F. C. Filament-Length-Controlled Elasticity in 3D Fiber Networks. *Phys. Rev. Lett.* **108,** 78102 (2012).
31. Heussinger, C. & Frey, E. Role of architecture in the elastic response of semiflexible polymer and fiber networks. *Phys. Rev. E* **75,** 11917 (2007).
32. Bouzid, M., Colombo, J., Barbosa, L. V. & Del Gado, E. Elastically driven intermittent microscopic dynamics in soft solids. *Nat. Commun.* **8,** 15846 (2017).
33. Bantawa, M. Hardening and softening materials: the role of network topology in soft gels. in *APS March Meeting 2018* (2018).
34. Evans, D. J. & Morriss, O. P. Non-Newtonian molecular dynamics. *Comput. Phys. Reports* **1,** 297–343 (1984).
35. Doi, M. Liquid crystals. in *Soft Matter Physics* 74–92 (Oxford Univ. Press, 2013).
36. Rheometer. *Universität Stuttgart - Institute of Physical Chemistry - Stubenrauch Group* (2017). Available at: http://www.ipc.uni-stuttgart.de/AKStubenrauch/research/equipment/rheometer/. (Accessed: 22nd December 2017)